

Signatures of Galactic Superwinds: Inhomogeneous Metal Enrichment of the Lyman Alpha Forest

Renyue Cen¹, Kentaro Nagamine² and Jeremiah P. Ostriker³

ABSTRACT

We investigate possible signatures of feedback from galactic superwinds on the metallicity of the Ly α forest, using a set of high resolution hydrodynamic simulations of a Λ cold dark matter model. Simulations produce metals self-consistently, based on one single parameter, the metal yield, which in turn is constrained by metallicity in the intra-cluster gas. We follow metals as a separate density species. For the metallicity of Ly α clouds with column density of $N_{HI} \sim 10^{14.5} - 10^{15.5} \text{ cm}^{-2}$ at $z = 2 - 4$ we find reasonable agreement between simulations, both with and without GSW, and observations (Schaye et al.). A unique signature and sensitive test of GSW is, however, provided by lower density regions with gas density of $\rho/\langle\rho\rangle = 0.01 - 1.0$ and a corresponding column density of $10^{12} - 10^{14} \text{ cm}^{-2}$. Without GSW we predict that both the mean and median metallicity of Ly α clouds in this column density range at $z = 2 - 4$ should have $Z \leq 10^{-3} Z_{\odot}$, since these small systems support little star formation. GSW contaminate these regions, however, and also there is a significant fraction ($\sim 25\%$) of Ly α clouds in this column density range which have a high metallicity excess of $10^{-2} Z_{\odot}$, resulting in a mean metallicity of $\sim 10^{-2} Z_{\odot}$. In addition, we find that there is a minimum in the median metallicity for clouds of $N_{HI} \sim 10^{13} - 10^{14} \text{ cm}^{-2}$ in the case with GSW, whereas without GSW the metallicity decreases monotonically and rapidly with decreasing column density. Finally, we predict that the ratio of secondary (e.g., N) to primary metals (e.g., O,C) is expected to be smaller by a factor of 10 in clouds of $N_{HI} \sim 10^{14.5} \text{ cm}^{-2}$ compared to that in large galaxies; this factor increases to ≥ 50 for $N_{HI} \leq 10^{13.5} \text{ cm}^{-2}$.

Subject headings: Cosmology: large-scale structure of Universe – cosmology: theory – intergalactic medium – quasars: absorption lines – hydrodynamics

¹Princeton University Observatory, Princeton University, Princeton, NJ 08544; cen@astro.princeton.edu

²Harvard-Smithsonian Center for Astrophysics, 60 Garden Street, Cambridge, MA 02138; knagamin@cfa.harvard.edu

³Princeton University Observatory, Princeton University, Princeton, NJ 08544; jpo@astro.princeton.edu

1. Introduction

Direct observational evidence for feedback from galactic superwinds (GSW) originating in starburst galaxies is ubiquitous both at low redshift (e.g., McCarthy, Heckman, & van Breugel 1987; Heckman, Armus, & Miley 1987; Papaderos et al. 1994; Marlowe et al. 1995; Lehnert & Heckman 1996; Bland & Tully 1988; Filippenko & Sargent 1992; Dahlem, Weaver, & Heckman 1998; Heckman et al. 1998; Martin 1999; Yoshida, Taniguchi, & Murayama 1999; Veilleux et al. 1999; Della Ceca et al. 1999; Veilleux, Shopbell, & Miller 2001; Rupke, Veilleux, & Sanders 2002; Martin, Kobulnicky, & Heckman 2002) and at high redshift (e.g., Franx et al. 1997; Pettini et al. 1998; Dawson et al. 2002; Pettini et al. 2001, 2002; Adelberger 2003; Adelberger et al. 2003). In addition, two lines of indirect but independent observational evidence point to the existence or need of GSW. First, the low-to-moderate density regions of the intergalactic medium (IGM) in Ly α clouds at $z \sim 2 - 3$ have already been enriched with metals to significant levels (e.g., Tytler et al. 1995; Songaila & Cowie 1996; Bergeron et al. 2002) to a level that would be difficult to achieve by sources embedded in those regions. And in the warm-hot intergalactic medium at low redshift (e.g., Tripp, Savage, & Jenkins 2000; Fang et al. 2002; Nicastro et al. 2002; Mathur, Weinberg, & Chen 2003) metals are seen that presumably originate from the galaxies central to these regions. Second, a substantial, non-gravitational heating source of the intra-cluster medium may be needed to produce the observed X-ray cluster luminosity-temperature relation and its evolution (e.g., Kaiser 1991; White 1991; David, Forman, & Jones 1991; Metzler & Evrard 1994; Navarro, Frenk, & White 1995; Pen 1999; Ponman, Cannon, & Navarro 1999; Balogh, Babul, & Patton 1999; Loewenstein 2000; Wu, Fabian, & Nulsen 2000; Lloyd-Davies, Ponman, & Cannon 2000; Brighenti & Mathews 2001; Neumann & Arnaud 2001; Borgani et al. 2001; Voit & Bryan 2001; Tozzi & Norman 2001; Davé et al. 2001; Babul et al. 2002; Bialek, Evrard, & Mohr 2001; McCarthy, Babul, & Balogh 2002; Afshordi & Cen 2002; Voit et al. 2002). GSW may play a significant role in the transport of metal-enriched matter to lower density regions outside galaxies and may help provide the requisite non-gravitational heating source for the cluster gas.

In contrast to notable successes of cosmological hydrodynamic simulations of the IGM that has not been intimately involved in star formation, such as the Lyman-alpha forest (Cen et al. 1994; Zhang et al. 1995; Hernquist et al. 1996; Miralda-Escudé et al. 1996; Bond & Wadsley 1997; Theuns et al. 1998), few calculations have been made to investigate the impact of GSW on the IGM in a coherent fashion. So far, most brute-force cosmological hydrodynamic simulations do not include the feedback effects of the GSW. For those simulations with GSW included (Cen, & Ostriker 1992, 1993a,b; Cen et al. 1994; Gnedin & Ostriker 1997; Gnedin 1998; Cen & Ostriker 1999b; Springel & Hernquist 2003; Kay et al. 2002; Theuns et al. 2002), the obtained results are often paradoxical; for

example, in very high resolution simulations dense regions tend to radiate away most of the GSW feedback energy and thus largely suppress its effect. This is for the most part due to the limited (and sometimes mismatched spatial and mass) numerical resolutions with the inability to properly represent, in cosmological simulations, a multi-phase ISM, where a GSW originates. On the other hand, simulations with lower resolution, limited by available computer power, but with a crude multi-phase medium treatment (e.g., Cen & Ostriker 1999a,b) appear to be able to exert substantial feedback energy on the general IGM surrounding galaxies. But the very limited resolution of these simulations does not allow us to draw reliable quantitative conclusions.

Although it is generally accepted that energy from collective supernova explosions and stellar winds should be powering the GSW (Ostriker & Cowie 1981; see Aguirre 1999 for a role that radiation pressure on dust plays in driving outflows), the complex structure of the interstellar medium (ISM) (McKee & Ostriker 1977) and the IGM makes quantitative calculations of GSW and subsequent evolution a daunting task, which certainly requires treatment of a multi-phase medium and may necessitate the explicit inclusion of magnetic fields (Koo & McKee 1992a,b; Smith 1996; Suchkov et al. 1996; Nath & Trentham 1997; Hartquist, Dyson, & Williams 1997; Gnedin & Ostriker 1997; Gnedin 1998; Mac Low & Ferrara 1999; Cen & Ostriker 1999b; Ferrara, Pettini, & Shchekinov 2000; Madau, Ferrara, & Rees 2001; Aguirre et al. 2001; Mori, Ferrara & Madau 2002; Scannapieco, Thacker, & Davis 2001; Scannapieco, Ferrara, & Madau 2002; Thacker, Scannapieco, & Davis 2002; White, Hernquist, & Springel 2002; Dyson, Arthur, & Hartquist 2002; Springel & Hernquist 2003). Significant progress has been made recently to provide a better treatment of the multi-phase interstellar medium (Yepes et al. 1997; Elizondo et al. 1999a,b; Hultman & Pharasyn 1999; Ritchie & Thomas 2001; Springel & Hernquist 2003) but the generation of GSW is far from being adequately modeled. Clearly, a combination of both high resolution and detailed multi-phase medium treatment (including magnetic fields and cosmic rays) is requisite before our understanding of the interactions between galaxy formation and IGM can be considered to be truly satisfactory.

But we will follow a somewhat different approach. We will not attempt to model the complex physics which determines how much of the SN energy produced within the galaxies can escape the galaxies. Rather we will inject energy directly into the medium surrounding the galaxies in a fashion that drives GSW and we will adjust the energy input to match the observed GSW. Direct and empirical determination of the output of energy and metal enriched gas from GSW is, in principle, possible (Chevalier & Clegg 1985), although, in practice, a complete account of the energy and mass output (especially the hot component at the X-ray band) from GSW may require more involved work (Strickland & Stevens 2000). Nevertheless, direct observational determinations of mass and energy loss rates from

GSW have yielded very interesting results (see Heckman 2001 for a recent review), with observations of both low redshift starburst galaxies and high redshift Lyman Break Galaxies (LBGs) indicating that both mass and energy outflows from GSW are comparable to those supplied by the interior starburst.

Thus, we accept at the outset our inability to correctly model the detailed structure of the ISM within these galaxies or the *generation* of the GSW. Rather, we will simply assume a proportionality between the star formation rate \dot{M}_* in the system and the output by that system of wind mass flux and energy flux, since there is a sound observational basis for this assumption. So we will assume that the energy *output* in a GSW is related to the star formation rate by $\dot{E}_{GSW} = e_{GSW}c^2\dot{M}_*$ (where c is the speed of light) and the mass output is $\dot{M}_{GSW} = \beta_{GSW}\dot{M}_*$. The two adjustable parameters (e_{GSW} , β_{GSW}) are then determined by a fit to observations (e.g., Pettini et al. 2001,2002; Heckman 2001), specifically, the two observed parameters - the mass flow rate and the wind velocity, and our subsequent computations are utilized to determine the *effects* of the consequent GSW on the metallicity distribution within the IGM, the shock-heating input to the IGM and the modification/regulation of subsequent galaxy formation. In brief, we seek to model the consequences not the causes of GSW feedback, and this is something that we think our codes are well designed to do. It should be stated that our approach is clearly incapable of fully solving the feedback process, since it is a phenomenological approach. But this is a major step forward to understand the effects of GSW, given the current state of knowledge which leaves the physics of generation of GSW largely unconstrained.

It may be useful to put this in a historical context. A decade ago the focus of cosmological simulations (e.g., Cen et al. 1994) was to fit the observed Ly α forest into the picture of modern hierarchical structure formation theory. The result was the emergence of the now standard theory for Ly α forest based on the growth/collapse of small scale density perturbations at moderate redshift. In this post-*WMAP* (*Wilkinson Microwave Anisotropy Probe*) era, research focus for Ly α forest has become to provide answers to the following question: how does galaxy formation affect the properties of Ly α forest and how is the power spectrum of primordial density fluctuation on small-scales reconstructed from Ly α forest flux distribution subject to various processes related to galaxy formation? This paper attempts to provide some partial answers to the first half of the question. In this first of a series of papers focusing on the effects of GSW on the IGM and subsequent galaxy/star formation, we will investigate the effect of GSW on the metal enrichment of the Ly α forest at high redshift ($z = 2 - 4$), which contains most of the mass as well as volume of the IGM then. The outline of this paper is as follows. The simulation details are given in §2. In §3 we give detailed results and we conclude in §4.

2. Simulations

Numerical methods of the cosmological hydrodynamic code and input physical ingredients have been described in detail in an earlier paper (Cen et al. 2003). We will name the code TIGER, **T**vd for **I**ntergalactic medium and **G**alaxy **E**volution and fo**R**mation. Briefly, the simulation integrates five sets of equations simultaneously: the Euler equations for gas dynamics, rate equations for different hydrogen and helium species at different ionization states, the Newton’s equations of motion for dynamics of collisionless particles, the Poisson’s equation for obtaining the gravitational potential field and the equation governing the evolution of the intergalactic ionizing radiation field, all in cosmological comoving coordinates. Note that the cosmological (frequency dependent) radiation field is solved for self-consistently, rather than being a separate input to the modeling. The gasdynamical equations are solved using the TVD (Total Variation Diminishing) shock capturing code (Ryu et al. 1993) on an uniform mesh. The rate equations are treated using sub-cycles within a hydrodynamic time step due to much shorter ionization time-scales (i.e., the rate equations are very “stiff”). Dark matter particles are advanced in time using the standard particle-mesh (PM) scheme. The gravitational potential on an uniform mesh is solved using the Fast Fourier Transform (FFT) method.

The initial conditions adopted are those for Gaussian processes with the phases of the different waves being random and uncorrelated. The initial condition is generated by the COSMICS software package kindly provided by E. Bertschinger (2001).

Cooling and heating processes due to all the principal line and continuum atomic processes for a plasma of primordial composition with additional metals ejected from star formation (see below), Compton cooling due to the microwave background radiation field and Compton cooling/heating due to the X-ray and high energy background are computed in a time-dependent, non-equilibrium fashion. The cooling due to metals is computed using a code based on the Raymond-Smith code (Raymond, Cox, & Smith 1976) assuming ionization equilibrium (Cen et al. 1995).

We follow star formation using a well defined prescription used by us in our earlier work (Cen & Ostriker 1992,1993) and similar to that of other investigators (Katz, Hernquist, & Weinberg 1992; Katz, Weinberg, & Hernquist 1996; Steinmetz 1996; Gnedin & Ostriker 1997). A stellar particle of mass $m_* = c_* m_{\text{gas}} \Delta t / t_*$ is created (the same amount is removed from the gas mass in the cell), if the gas in a cell at any time meets the following three conditions simultaneously: (i) contracting flow, (ii) cooling time less than dynamic time, and (iii) Jeans unstable, where Δt is the time step, $t_* = \max(t_{\text{dyn}}, 10^7 \text{yrs})$, $t_{\text{dyn}} = \sqrt{3\pi / (32G\rho_{\text{tot}})}$ is the dynamical time of the cell, m_{gas} is the baryonic gas mass in the cell and $c_* = 0.07$ is star formation efficiency. Each stellar particle has a number of other attributes at birth,

including formation time t_i , initial gas metallicity and the free-fall time in the birth cell t_{dyn} . The typical mass of a stellar particle in the simulation is about one million solar masses; in other words, these stellar particles are like coeval globular clusters.

Stellar particles are subsequently treated dynamically as collisionless particles. But feedback from star formation is allowed in three forms: ionizing UV photons, supernova kinetic energy (i.e., GSW), and metal-enrich gas, all being proportional to the local star formation rate. The temporal release of all three feedback components at time t has the same form: $f(t, t_i, t_{dyn}) \equiv (1/t_{dyn})[(t - t_i)/t_{dyn}] \exp[-(t - t_i)/t_{dyn}]$. Within a time step dt , the released GSW energy to the IGM, ejected mass from stars into the IGM and escape UV radiation energy are $e_{GSW} f(t, t_i, t_{dyn}) m_* c^2 dt$, $e_{mass} f(t, t_i, t_{dyn}) m_* dt$ and $f_{esc}(Z) e_{UV}(Z) f(t, t_i, t_{dyn}) m_* c^2 dt$. We use the Bruzual-Charlot population synthesis code (Bruzual & Charlot 1993; Bruzual 2000) to compute the intrinsic metallicity-dependent UV spectra from stars with Salpeter IMF (with a lower and upper mass cutoff of $0.1 M_\odot$ and $125 M_\odot$). Note that e_{UV} is no longer just a simple coefficient but a function of metallicity. The Bruzual-Charlot code gives $e_{UV} = (1.2 \times 10^{-4}, 9.7 \times 10^{-5}, 8.2 \times 10^{-5}, 7.0 \times 10^{-5}, 5.6 \times 10^{-5}, 3.9 \times 10^{-5}, 1.6 \times 10^{-6})$ at $Z/Z_\odot = (5.0 \times 10^{-3}, 2.0 \times 10^{-2}, 2.0 \times 10^{-1}, 4.0 \times 10^{-1}, 1.0, 2.5, 5.0)$. We also implement a gas metallicity dependent ionizing photon escape fraction from galaxies in the sense that higher metallicity hence higher dust content galaxies are assumed to allow a lower escape fraction; we adopt the escape fractions of $f_{esc} = 2\%$ and 5% (Hurwitz et al. 1997; Deharveng et al. 2001; Heckman et al. 2001) for solar and one tenth of solar metallicity, respectively, and interpolate/extrapolate using a linear log form of metallicity. In addition, we include the emission from quasars using the spectral form observationally derived by Sazonov, Ostriker, & Sunyaev (2004), with a radiative efficiency in terms of stellar mass of $e_{QSO} = 2.5 \times 10^{-5}$ for $h\nu > 13.6\text{eV}$. Finally, hot, shocked regions (like clusters of galaxies) emit ionizing photons due to bremsstrahlung radiation, which are also included. The UV component is simply averaged over the box, since the light propagation time across our box is small compared to the time steps. The radiation field (from 1eV to 100keV) is followed in detail with allowance for self-consistently produced radiation sources and sinks in the simulation box and for cosmological effects, i.e., radiation transfer for the mean field J_ν is computed with stellar, quasar and bremsstrahlung sources and sinks due to Ly α clouds etc. In addition, a local optical depth approximation is adopted to crudely mimic the local shielding effects: each cubic cell is flagged with six hydrogen “optical depths” on the six faces, each equal to the product of neutral hydrogen density, hydrogen ionization cross section and scale height, and the appropriate mean from the six values is then calculated; equivalent ones for neutral helium and singly-ionized helium are also computed. In computing the global sink terms for the radiation field the contribution of each cell is

subject to the shielding due to its own “optical depth”. In addition, in computing the local ionization and cooling/heating balance for each cell the same shielding is taken into account to attenuate the external ionizing radiation field.

GSW energy and ejected metals are distributed into 27 local gas cells centered at the stellar particle in question, weighted by the specific volume of each cell. We fix $e_{mass} = 0.25$. GSW energy injected into the IGM is included with an adjustable efficiency (in terms of rest-mass energy of total formed stars) of e_{GSW} , which is normalized to observations for our fiducial simulation with $e_{GSW} = 3 \times 10^{-6}$. If the ejected mass and associated energy propagate into a vacuum, the resulting velocity of the ejecta would be $(2e_{GSW}/e_{mass})^{1/2}c = 1469\text{km/s}$. After the ejecta has accumulated an amount of mass comparable to its initial mass, the velocity may slow down to a few hundred km/s. We assume this velocity would roughly correspond to the observed outflow velocities of LBGs (e.g., Pettini et al. 2002). We also make simulations with no GSW and with stronger GSW to investigate the effects of GSW on IGM.

We do not separately make any adjustments to fit to the observed distributions and evolution of metals, but assume a specific efficiency of metal formation, an “yield” (Arnett 1996), $y_0 = 0.02$, the percentage of stellar mass that is ejected back into IGM as metals. We note that $y_0 = Z_{ejecta}e_{mass}$; since $y_0 = 0.02$ and $e_{mass} = 0.25$, it implies that the ejecta metallicity is $Z_{ejecta} = 0.08 = 4Z_{\odot}$. Metals in the IGM (assuming the standard solar composition) are followed as a separate variable (analogous to the total gas density) with the same hydrocode. In addition, we implement another density variable to keep track of the reprocessed, i.e., secondary metals in the ejecta, which is proportional to the metallicity of the gas from which the star was formed.

Since we are interested in the metallicity of the IGM, it is legitimate to question whether our adopted constant metal yield is reasonable. We can not answer this question from first principles. Rather, we will consider a physically motivated case, where the metallicity yield is a function of gas metallicity out of which stars are formed. It is thought that the initial mass function of stars formed out of low metallicity gas may contain relatively more high mass stars thus produce a higher yield (for references to the original literature see Ricotti & Ostriker 2004). We adopt this view and consider a scenario with varying yield by making a correction to the computed yield as described below. We present results for both the case of constant yield and metallicity dependent yield to indicate the uncertainties and/or adjustability of the results.

Let the yield be $y(Z)$. It can then be shown that the final corrected metallicity of a region with computed metallicity Z_c will be $Z_v = Z_c y(Z_c)/(y_0 f(Z_c))$, where $f(Z_c) = (y(Z_c)/Z_c) \int_0^{Z_c} dx/y(x)$. We somewhat arbitrarily set the form of $y(Z)$ to be

$y(Z) = (5.0 + 45.0(1 - \exp(-Z/B))^{-1}$, which gives $y = 0.02$ for $Z \gg B$ and $y = 0.2$ for $Z \ll B$. Thus we have adopted a higher yield of 0.2 for metal-free stars, which may be a reasonable choice if IMF of metal-free stars are top-heavy (Woosley & Weaver 1995). The transition metallicity B is uncertain but we use $10^{-3} Z_{\odot}$ for the illustration (Bromm & Loeb 2003; Fang & Cen 2004).

The results reported on here are based on new simulations of a *WMAP*-normalized (Spergel et al. 2003) cold dark matter model with a cosmological constant: $\Omega_M = 0.29$, $\Omega_b = 0.047$, $\Omega_{\Lambda} = 0.71$, $\sigma_8 = 0.85$, $H_0 = 100h\text{kms}^{-1}\text{Mpc}^{-1} = 70\text{kms}^{-1}\text{Mpc}^{-1}$ and $n = 1.0$. Seven simulations with varying box size, resolution and input physics are made, as listed in Table 1. Mass resolution is extremely important for an analysis of this type as it is the lowest mass systems in relatively low density regions that contain the stars which are most suitable for contamination of the low and moderate density IGM. The mass resolutions are considerably better than those of most cosmological simulations, but the spatial resolution, while significantly inferior to that obtained in both the SPH and AMR schemes, is, we believe, adequate for the present purpose. The coarser spatial resolution among the listed simulations is smaller than the Jeans length of photoionized IGM at $z = 2 - 4$ by a factor greater than 10 but only marginally resolve some small galaxies of total mass $10^9 M_{\odot}$. But our higher resolution simulation indicates that results are not significantly affected.

The first simulation (N432L11M) is our fiducial one with a GSW feedback that is approximately matched to observations of Lyman break galaxies. The second simulation (N432L11L) has negligible GSW, while the third simulation (N432L11H) has GSW energy that is higher than the fiducial run by a factor of 5. The higher resolution run (N864L11M) has twice as high spatial resolution but with all other physics fixed the same and is made to check the dependence of the results on the resolution and the convergence of the results on resolution. As will be shown below, a proper convergence has been achieved for the problem in hand. The larger simulation (N864L22M) is made to check the dependence of the results on the box size and, as one would have expected, the $11h^{-1}\text{Mpc}$ box seems adequate for the objects under investigation at high redshift. The last two simulations (N432L11M8 and N432L11M32) have the exact same input physics and resolutions as the fiducial run but with the initial power spectrum cutoff at 8 and 32 cells, respectively, instead of 2 cells in the fiducial run. These two runs were made with the purpose of isolating some of the effects due to small galaxies forming from density fluctuations of high wave numbers.

The program used to generate synthetic Ly α forest lines here is the same one used in our previous papers (Cen et al. 1994; Miralda-Escudé et al. 1996). The only addition is that we have in addition the metal density, which allows detailed computations of metallicity distributions in the Ly α forest. All transmitted flux is computed with a FWHM

Table 1. A List of Simulations

| Run | Label | Box | Spatial Res | Mass Res | k_{max} | e_{GSW} |
|-----|------------|----------------------|----------------------|-----------------------------|-----------------------|----------------------|
| 1 | N432L11M | $11h^{-1}\text{Mpc}$ | $25h^{-1}\text{kpc}$ | $2.1 \times 10^5 M_{\odot}$ | $123h\text{Mpc}^{-1}$ | 3×10^{-6} |
| 2 | N432L11L | $11h^{-1}\text{Mpc}$ | $25h^{-1}\text{kpc}$ | $2.1 \times 10^5 M_{\odot}$ | $123h\text{Mpc}^{-1}$ | 0 |
| 3 | N432L11H | $11h^{-1}\text{Mpc}$ | $25h^{-1}\text{kpc}$ | $2.1 \times 10^5 M_{\odot}$ | $123h\text{Mpc}^{-1}$ | 1.5×10^{-5} |
| 4 | N864L11M | $11h^{-1}\text{Mpc}$ | $13h^{-1}\text{kpc}$ | $2.7 \times 10^4 M_{\odot}$ | $123h\text{Mpc}^{-1}$ | 3×10^{-6} |
| 5 | N864L22M | $22h^{-1}\text{Mpc}$ | $25h^{-1}\text{kpc}$ | $2.1 \times 10^5 M_{\odot}$ | $123h\text{Mpc}^{-1}$ | 3×10^{-6} |
| 6 | N432L11M8 | $11h^{-1}\text{Mpc}$ | $25h^{-1}\text{kpc}$ | $2.1 \times 10^5 M_{\odot}$ | $31h\text{Mpc}^{-1}$ | 3×10^{-6} |
| 7 | N432L11M32 | $11h^{-1}\text{Mpc}$ | $25h^{-1}\text{kpc}$ | $2.1 \times 10^5 M_{\odot}$ | $7.7h\text{Mpc}^{-1}$ | 3×10^{-6} |

Note. — The first and second columns give a numeric number for each run and a label indicating the number of cells used (432 for 432^3 cells and 864 for 864^3 cells), the box size ($11h^{-1}\text{Mpc}$ and $22 h^{-1}\text{Mpc}$) and the level of GSW (‘L’ for low, ‘M’ for median, and ‘H’ for high). The simulations labeled with $N432$ have 216^3 dark matter particles, whereas those labeled with $N864$ have 432^3 dark matter particles. Box sizes (third column) and spatial resolution (fourth column) are both in comoving units. The fifth column is the mean baryonic cell mass; the corresponding dark matter particle mass is $1.0 \times 10^7 M_{\odot}$ for Runs (1,2,3,5,6,7) and $1.3 \times 10^6 M_{\odot}$ for Run 4. The initial maximum wavenumber k_{max} (sixth column) for the input power spectrum is in comoving $h\text{Mpc}^{-1}$. The last column indicates the GSW strength.

of 6.6kms^{-1} , a sample pixel size of 2kms^{-1} and Gaussian noise added to each pixel with a signal-to-noise ratio of 150. Mean decrement is chosen to match $\bar{D} = 0.34$ (e.g., Press, Rybicki, & Schneider 1993) in all simulated spectra by adjusting the background radiation field to facilitate a meaningful comparison.

3. Results

Figure 1 shows the distributions of IGM temperature for a typical slice of the indicated size. The left panel is with GSW (Run 1: N432L11M) and the right panel without GSW (Run 2: N432L11L). It is clear that GSW do blow bubbles of hot gas, which occupy a radius typically of hundreds of kpc.

Before proceeding to compute the metallicity distribution in the Ly α forest, it is pertinent to ask if a substantial GSW feedback on the IGM may spoil the excellent agreement found between the predictions of the cold dark matter model and the observed Ly α forest (Cen et al. 1994; Zhang et al. 1995; Hernquist et al. 1996; Miralda-Escudé et al. 1996; Rauch et al. 1997; Croft et al. 1999; McDonald et al. 2000). The recent work of Theuns et al. (2002) has clearly demonstrated that GSW mainly propagate in the directions of lowest column density, and filaments (producing most of the Ly α forest) are not significantly affected by GSW. They show quantitatively that Ly α forest statistics such as column density distribution and Doppler width distribution remain little changed and the good agreement between cold dark matter model and observations is, to the zero-th order, unaltered by GSW to the concerned accuracies. Here we will confirm their conclusions. Figure 2 visually presents this point, showing little alteration of the density distributions in filaments. A joint examination of Figures 1,2 indicates that GSW prefer to travel in the directions roughly perpendicular to the filaments, as found by Theuns et al. (2002).

To further demonstrate that GSW do not significantly alter the flux distribution of the Ly α forest, Figure 3 shows the probability distributions of transmitted flux fraction, defined as $F \equiv \exp(-\tau)$, for the seven runs tabulated in Table 1. The fact that all the runs, except Runs 5 (N864L22M) and 7 (N432L11M32), nearly overlay with one another clearly shows that the effect of GSW on flux distribution and other derived quantities (such as column density distribution, etc.,) will remain relatively unaltered, retaining the previous good agreement found between simulations and observations. The fact that the higher resolution run (Run 4: N864L11M) agrees with lower resolution runs (Runs 1,2,3: N432L11M, N432L11L, N432L11H) suggests that our fiducial run (Run 1: N432L11M) has adequate resolution. The deviation of Run 5 (N864L22M) from the rest is due to cosmic variance, while the deviation of Run 7 (N432L11M32) from the rest is a result of missing

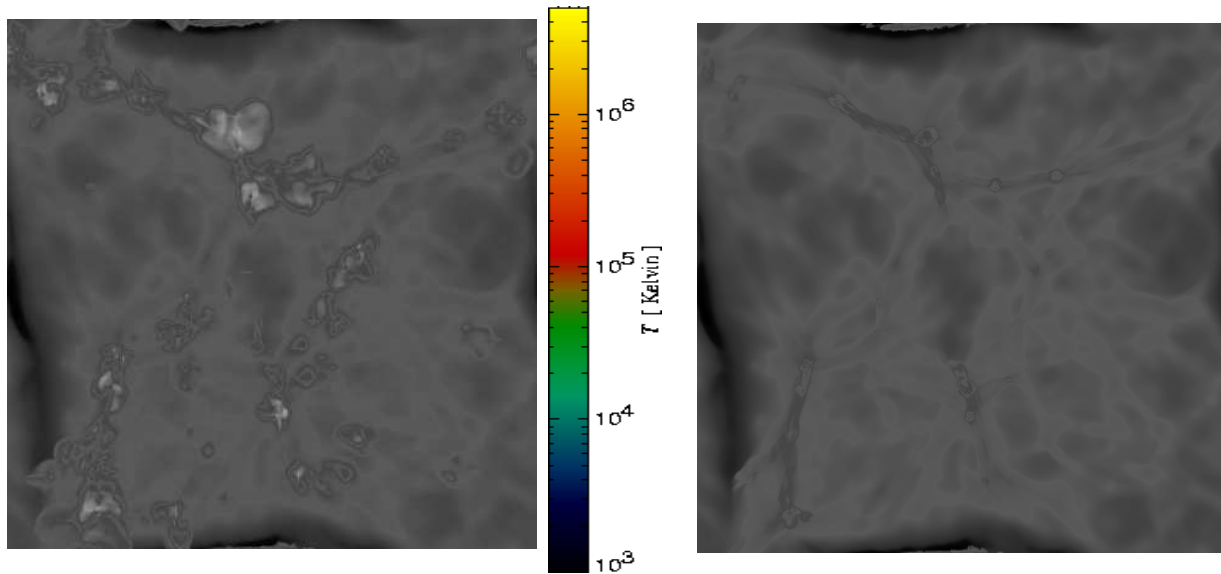


Fig. 1.— Projected temperature of a slice of size $11 \times 11 h^{-2} \text{Mpc}^2$ comoving and a depth of $2.75 h^{-1} \text{Mpc}$ comoving at redshift $z = 3$ with (left panel) and without (right) GSW, respectively. The strength of the GSW is normalized to LBG observations.

small-scale power in that run.

However, the fact that GSW do propagate some distance, especially into the low density

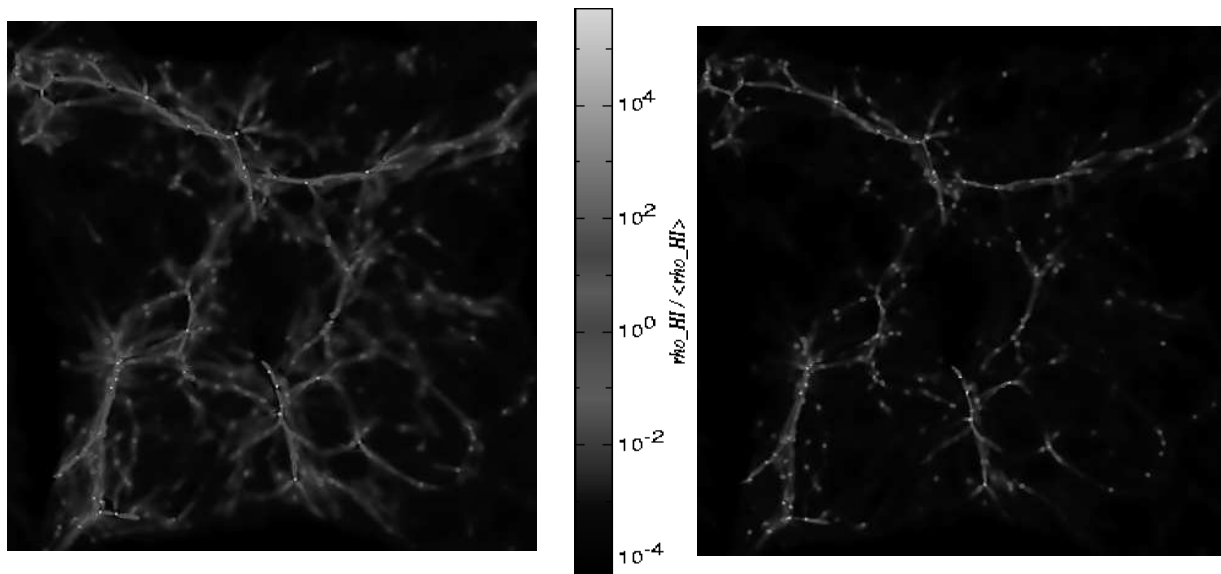


Fig. 2.— Projected neutral hydrogen overdensity of the same slice as in Figure 1 with (left panel) and without (right) GSW, respectively.

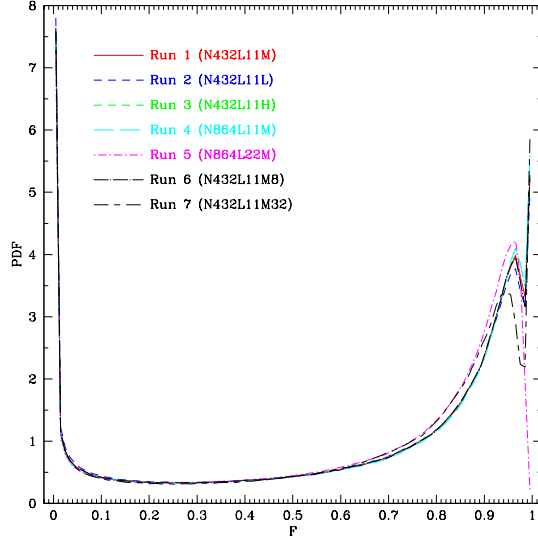


Fig. 3.— shows the flux probability distribution function (PDF) for the seven runs at $z = 3$.

regions, as shown in Figure 1, suggests that some low column density Ly α clouds should

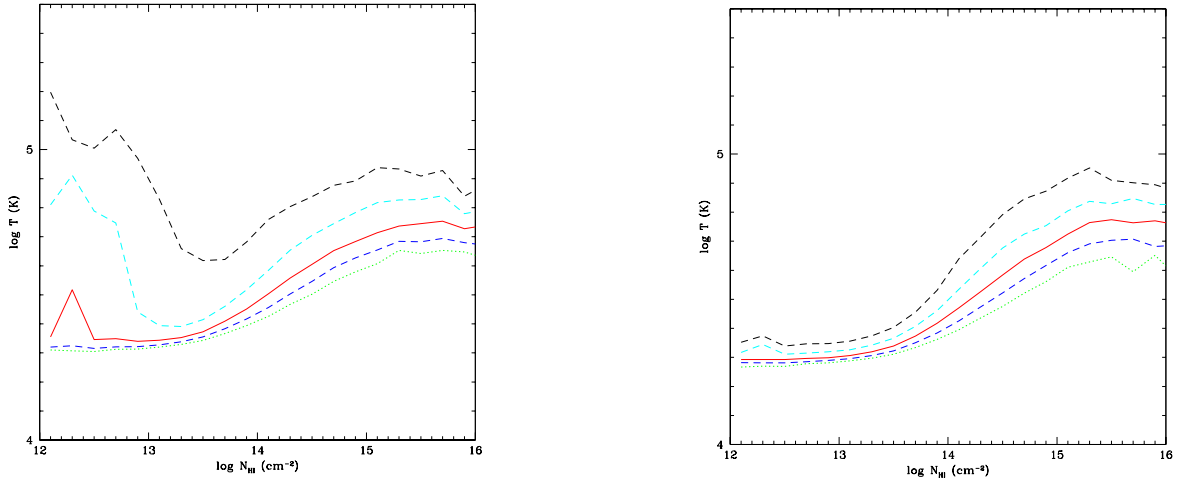


Fig. 4.— shows the temperature as a function of Ly α cloud column density for the two cases with (left panel; Run 1:N432L11M) and without (right panel; Run 2:N432L11L) GSW, respectively, at $z = 3$. The five curves in each panel correspond to 10%, 25%, 50%, 75%, 90% percentiles; i.e., 10% of clouds has a temperature below the bottom curve, while 90% of clouds has a temperature below the top curve, etc.

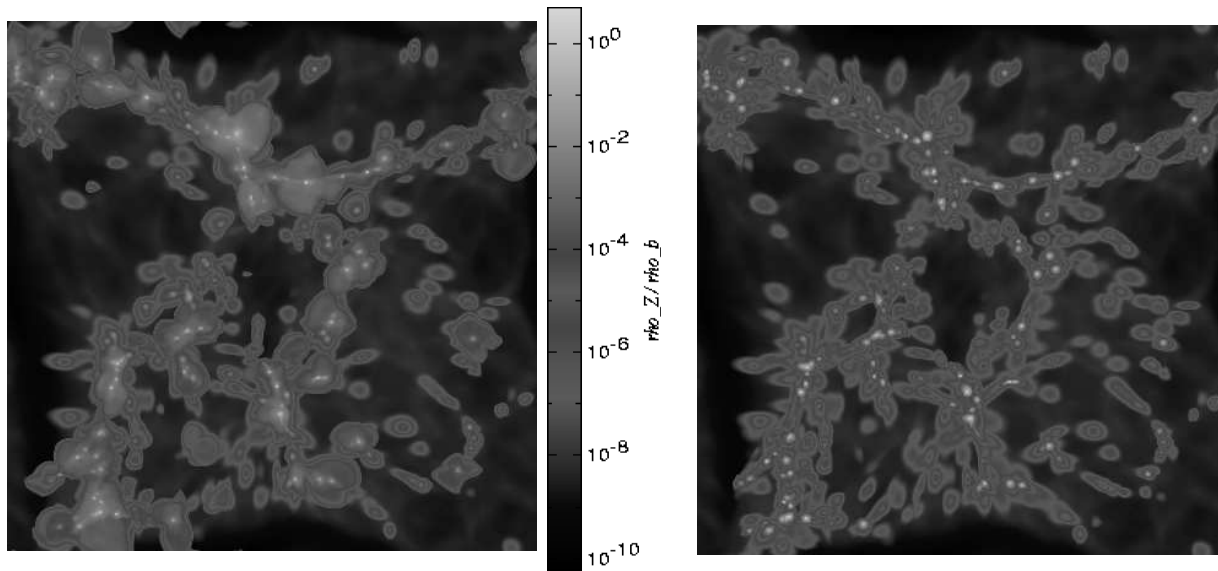


Fig. 5.— Projected metallicity of a slice of size $11 \times 11 h^{-2} \text{Mpc}^2$ comoving and a depth of $2.75 h^{-1} \text{Mpc}$ comoving at redshift $z = 3$ for a *WMAP*-normalized ΛCDM model with (left panel) and without (right) GSW, respectively. The strength of the GSW is normalized to LBG observations. This is the same slice as in Figure 1.

be affected to varying degrees. Figure 4 shows the temperature as a function of $\text{Ly}\alpha$ cloud column density for the two cases with (left panel; Run 1: N432L11M) and without (right panel; Run 2: N432L11L) GSW, respectively. It is evident that, while $\text{Ly}\alpha$ clouds with column density $N_{\text{HI}} \geq 10^{14} \text{cm}^{-2}$ are only affected modestly, those with $N_{\text{HI}} \leq 10^{14} \text{cm}^{-2}$ are increasingly affected. A closer examination suggests that roughly 25% of clouds with $N_{\text{HI}} \leq 10^{14} \text{cm}^{-2}$ is seen to experience significant heating by the GSW, and the effect decreases towards higher columns. However, we have checked the cloud velocity width distributions with the and without GSW and do not find noticeable differences, suggesting an overall domination of peculiar velocities in broadening clouds. Combining observations of hydrogen lines with metal lines, which suffer less thermal broadening, however, may allow one to see the GSW heating effect in the low column density $\text{Ly}\alpha$ forest, at least for some individual cases with low peculiar velocity broadening.

Let us now turn to the main point of the paper. Could the GSW transport metal enriched gas to raise the metallicity of low density regions to a level consistent with the observed metallicity? Are there palpable signatures of GSW on $\text{Ly}\alpha$ forest? Figure 5 shows the spatial distribution of metallicity in the IGM with (left panel) and without (right panel) GSW. It is visible from Figures 5 that, while other, gravitational (e.g., Gnedin 1998) and hydrodynamic processes do transport metals to the vicinity ($\leq \sim 100 \text{kpc}$) of galaxies without

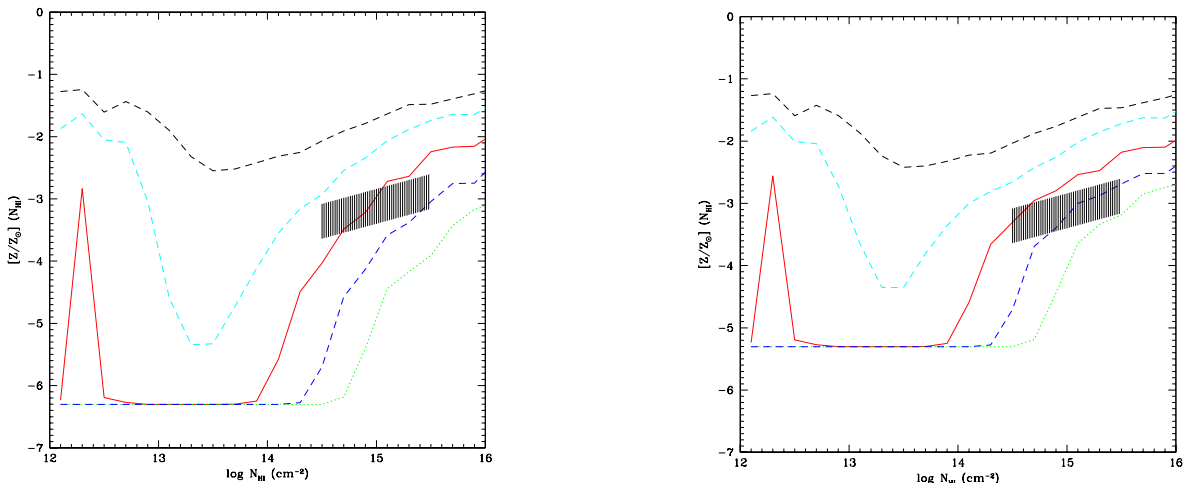


Fig. 6.— shows the metallicity as a function of Ly α cloud column density for Run 1 (N432L11M) with two cases of metal yields: left panel with constant yield $y_0 = 0.02$ and right panel with varying yield with a transition to higher yield at $Z = 10^{-3} Z_{\odot}$, at $z = 3$. The five curves in each panel correspond to 10%, 25%, 50%, 75%, 90% percentiles. The shaded regions indicate the observed median metallicity as a function of column density from Schaye et al. (2003) with 1σ bounds.

GSW (right panel of Figure 5), GSW appear to play a more important role to transport the metals from galaxies to larger distances, in conjunction with other, gravitational and non-gravitational processes. The “metal bubbles” (reddish bubbles seen in the left panel of Figure 5) have $\rho_{metals}/\rho_{gas} \sim 10^{-4}$, indicating that these metal-contaminated regions are enriched to a metallicity close to $10^{-2} Z_{\odot}$.

Figure 6 shows the metallicity as a function of Ly α cloud column density for our fiducial run (Run 1: N432L11M) with two yield schemes. For the clouds within the range of column densities ($N_{HI} \sim 10^{14} - 10^{15} \text{cm}^{-2}$), where comparisons with observations can be made, it is very encouraging that the agreement between observations and simulations is good, considering that our simulations have essentially only one free parameter for the metal yield, which in turn is fixed based on theory of stellar interior and turns out also to be required to match the metallicity of the intra-cluster gas (Arnaud et al. 1994; Mushotsky et al. 1996; Mushotsky & Lowenstein 1997; Cen & Ostriker 1999b). A comparison between the left and right panels suggests that, if there is a transition such that the metal yield from stars is significantly higher for nearly metal free gas, it seems that the transition is likely to have occurred at $Z \leq 10^{-3} Z_{\odot}$, perhaps at $Z \sim 10^{-4} - 10^{-3} Z_{\odot}$; a transition at a higher gas metallicity would over-enrich the IGM at the relevant densities.

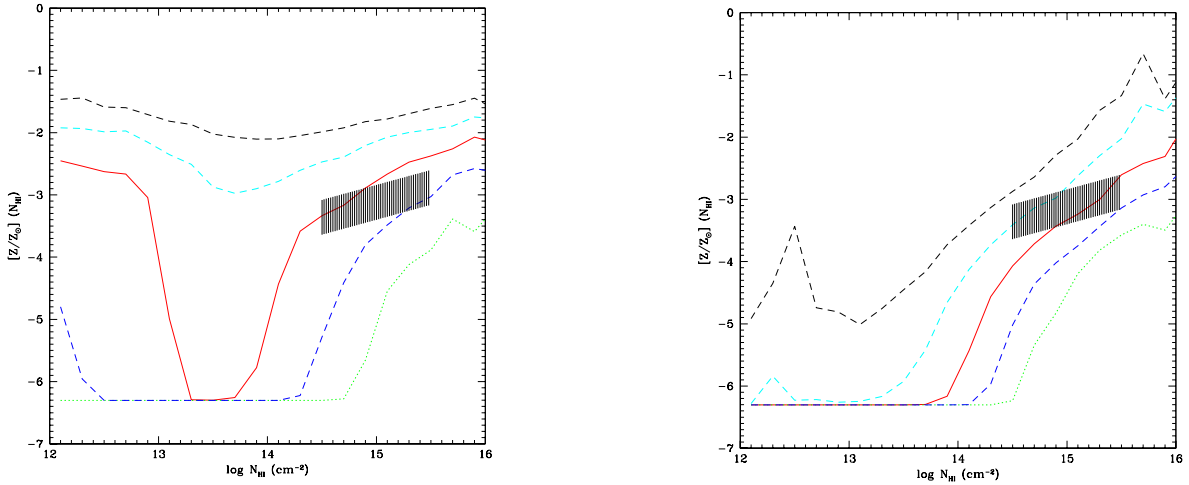


Fig. 7.— shows the metallicity as a function of Ly α cloud column density for Run 3 (N432L11H, left panel) and Run 2 (N423L11L, right panel) with constant metal yield, at $z = 3$. The five curves in each panel correspond to 10%, 25%, 50%, 75%, 90% percentiles. The shaded regions indicate the observed median metallicity as a function of column density from Schaye et al. (2003) with 1σ bounds.

How sensitive are the results to the strength of GSW? Figure 7 shows the cases with GSW strength (energy) five times stronger than the fiducial run (left panel) and with no GSW (right panel). We see that both these cases are consistent with observations. This is because the Ly α clouds with column densities in the range examined, where metallicity can be observationally accurately determined, are mostly located in the filaments somewhat further away from galaxies and not substantially affected by GSW, consistent with Figure 3. This indicates the metallicity of gas in Ly α clouds with column density in the range $N_{HI} = 10^{14.5} - 10^{15.5} \text{cm}^{-2}$ mainly reflects the *local* star formation history. Some effect of GSW is seen in the sense that higher GSW produces somewhat higher metallicity for the Ly α clouds in that column density range, but the differences are comparable to observational uncertainties. As it turns out, metallicity of Ly α clouds in the column density range of $N_{HI} = 10^{14.5} - 10^{15.5} \text{cm}^{-2}$ provides an insensitive test of GSW (see Figure 8 for a further demonstration).

A more powerful discriminant may lie in the metallicity of lower column density clouds, to some of which GSW are able to transport metals, as visually seen in Figures (1,5). A closer comparison between left panels of Figures 6,7 (with GSW) and right panel of Figure 7 (without GSW) already reveals this signature: *there are dramatic differences at $N_{HI} \leq 10^{13.5} \text{cm}^{-2}$, between simulation with GSW and without*

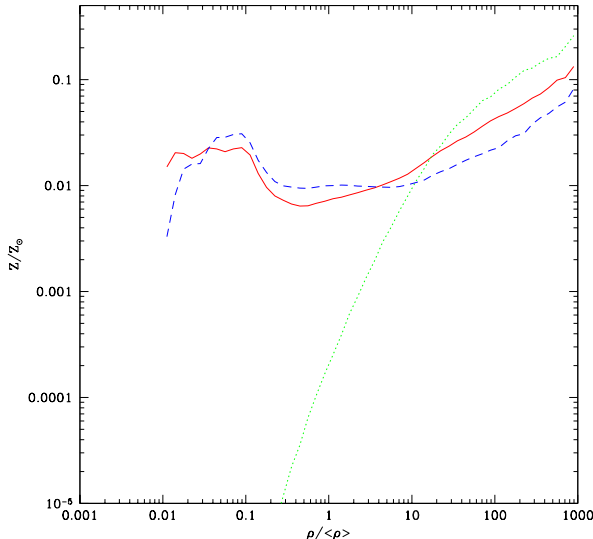


Fig. 8.— shows mean metallicity as a function of gas density for three runs: fiducial with realistic GSW (Run 1:N432L11M; solid curve), high GSW run (Run 3:N432L11H; dashed curve) and no GSW run (Run 2:N432L11L, dotted curve) at $z = 3$.

GSW, where $N_{HI} = 10^{13.5}\text{cm}^{-2}$ approximately corresponds to $\rho/\langle\rho\rangle \leq 1$ at $z = 3$, using the formula relating column density to gas density in Schaye et al. (2003), $\rho/\langle\rho\rangle = 10(N_{HI}/10^{15}\text{cm}^{-2})^{2/3}[(1+z)/4]^{-3}$. Apparently GSW are able to transport metals to some low density regions within which embedded star formation was inefficient, presumably in directions roughly perpendicular to the filaments as seen in Figures (1,5). In the fiducial run with GSW (Run 1: N432L11M) there are about 25% of Ly α clouds with $N_{HI} < 10^{13}\text{cm}^{-2}$ may have metallicity in excess of $10^{-2} Z_{\odot}$, whereas there is none in the run without GSW.

To elucidate this physical point, in Figure 8, we plot the mean metallicity as a function of gas density. We see the expected but now precisely quantified difference between runs with GSW (solid and dashed curves) and without GSW (dotted curve): GSW are able to transport metals to regions at $\rho/\langle\rho\rangle < 10$, whereas without GSW most of the metals are trapped in regions with $\rho/\langle\rho\rangle > 10$. The mean metallicity is larger by a factor of (7, 40, 500) at $\rho/\langle\rho\rangle = (3, 1, 0.1)$ in Run 1 (N432L11M) than in Run 2 (N432L11L), with the difference becoming still larger at lower $\rho/\langle\rho\rangle < 0.1$. We see that without GSW mean metallicity is a steep monotonic function of density, whereas with GSW there two are peaks, where the lower metallicity peak at $\rho = (0.01 - 0.1)\langle\rho\rangle$ represents metal enriched low density regions, a signature of GSW, consistent with Figures (6,7). This is the most clear demonstration of the GSW effect on the metal enrichment of the IGM and a clear signature of GSW:

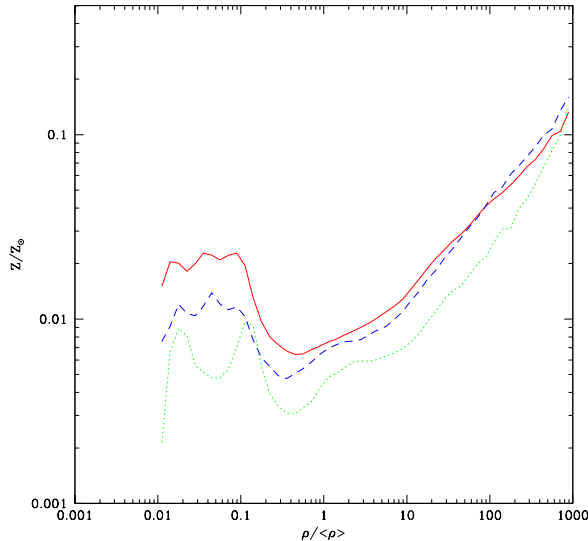


Fig. 9.— shows mean metallicity as a function of gas density for three runs: fiducial run with realistic GSW (Run 1:N432L11M; solid curve), reduced small-scale power run at 8 cells (Run 6:N432L11M8; dashed curve) and reduced small-scale power run at 32 cells (Run 7:N432L11M32; dotted curve).

with increasing observational sensitivity one should expect to see the metallicity at lower density regions $\rho/\langle\rho\rangle < 1$ increasing rather than decreasing. The existence of a metallicity trough at $N_{HI} = 10^{13-14}\text{cm}^{-2}$ (Figures 6, 7) or $\rho/\langle\rho\rangle = 0.1 - 1$ (Figure 8) in the simulations with GSW is a clear indication that GSW propagate anisotropically; in other words, some intermediate density region along filaments are relatively less affected. We note that metal enrichment from galaxies not resolved in our simulations (a few times $10^7 M_{\odot}$) at earlier epochs is unlikely to be important compared to the observed levels, as shown by Norman, O’Shea, & Paschos (2004), but may put a somewhat higher metallicity floor for the case without GSW.

What galaxies are responsible for transporting metals to the low density regions? Figure 9 shows a comparison between Runs 1,6,7 (N432L11M, N432L11M8, N432L11M32). These vary in their high wavenumber cutoff corresponding to minimum halo mass $M_{min} \sim (\pi/k_{max})^3 \langle\rho\rangle$ of $1.1 \times 10^7 h^{-1} M_{\odot}$, $7.0 \times 10^8 h^{-1} M_{\odot}$, $4.5 \times 10^{10} h^{-1} M_{\odot}$, in Run 1 (N432L11M), 6 (N432L11M8) and 7 (N432L11M32), respectively. We see that, while the difference at $\rho/\langle\rho\rangle \sim 10^3$ where large galaxies are located is small between the runs, the difference between Run 1 (N432L11M) and Run 7 (N432L11M32) is about 2.5 – 5.0 and the difference between Run 1 (N432L11M) and Run 6 (N432L11M8) is about 2 at the low metallicity peak at $\rho/\langle\rho\rangle \sim 0.01 - 0.1$. A simple interpretation of Figure 9 is that galaxies

with mass in the range $(1.1 \times 10^7 h^{-1} - 4.5 \times 10^{10}) h^{-1} M_{\odot}$ all contribute to the metal enrichment of the lower density IGM, with approximately 25% from $> 4.5 \times 10^{10} h^{-1} M_{\odot}$, 50% from $7.0 \times 10^8 - 4.5 \times 10^{10} h^{-1} M_{\odot}$ and 25% from $< 7.0 \times 10^8 h^{-1} M_{\odot}$. The recent work by Aguirre et al. (2001) has shown that massive galaxies at low redshift are not very effective in enriching the IGM to a relatively uniform degree. On the other hand, GSW from dwarf galaxies at high redshift appear to be able to more effectively disperse metals relatively uniformly without traveling a very long distance (e.g., Schwarz, Ostriker, & Yahil 1975; Cen & Bryan 2001; Madau, Ferrara, & Rees 2001). Our results are fully consistent with these earlier works. We further analyze the simulations by removing a sphere of radius $1 h^{-1} \text{Mpc}$ around each simulated Lyman Break Galaxy, identified as galaxies brighter than rest-frame V -band magnitude $M_V = -21$, as most of the brightest galaxies in the simulation satisfy the color-color selection criteria of LBGs used by observers (e.g. Nagamine 2002; Nagamine et al. 2004a,b). The results (not shown) in a similar plot to Figure 6 are virtually identical to Figure 6. This indicates that the contribution from ongoing star forming massive galaxies is, as expected, negligible, simply because there is a lag due to finite GSW propagation time. This is also in part because the massive galaxies do not make large contribution to metal enrichment of the low density IGM, consistent with Figure 9 and earlier results of Aguirre et al. (2001).

To better understand responsible galaxies for the metal enrichment of Ly α forest, Figure 10 shows the ratio of mean secondary metallicity to mean primary metallicity as a function of column density. Within galaxies, the ratio of secondary to primary metals is proportional to the ratio primary/hydrogen. Thus higher values of S/P indicate an origin of metals in more massive, more metal rich systems. The most striking feature in this figure is the dramatic decrease of the ratio from ~ 1 in the highest column density clouds to about 0.003 – 0.02 in the low column density clouds, a drop of a factor of 50 – 300, for the fiducial model (red curve). Quantitatively, we see that the ratio of secondary (e.g., N) to primary metals (e.g., O,C) is expected to be smaller by a factor of 10 in clouds of $N_{HI} \sim 10^{14.5} \text{cm}^{-2}$ compared to that in large galaxies and by a factor of ≥ 50 for $N_{HI} \leq 10^{13.5} \text{cm}^{-2}$. This can be most easily understood and consistent with Figure 9, if most of the metal enrichment of Ly α forest is due to dwarf galaxies (Dekel & Silk 1986; Mac Low & Ferrara 1999; Madau, Ferrara, & Rees 2001), where gas retainment is more difficult and thus metal recycling is limited.

Some other interesting features are also present in Figure 10. A comparison among the red solid, blue long-dashed (with GSW) and green dotted curves (no GSW) reveals a couple of noticeable properties. First, the runs with GSW show an upturn of the ratio at $N_{HI} < 10^{13.5} \text{cm}^{-2}$, although the level is still a factor of 50 – 100 below the high density regions. The fact there is an upturn and a valley at $N_{HI} \sim 10^{13.5} \text{cm}^{-2}$ shows that the

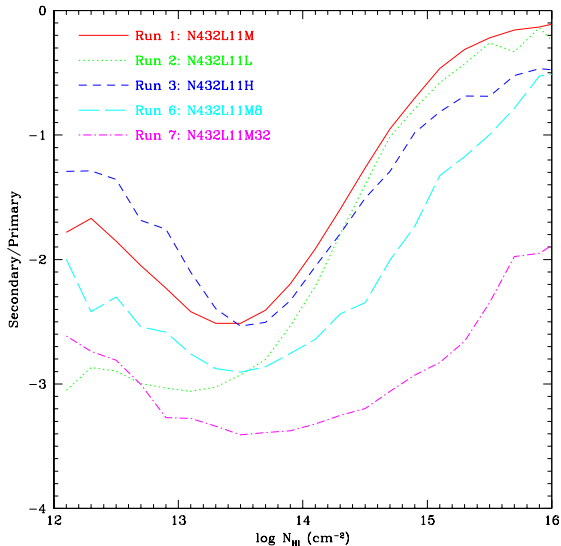


Fig. 10.— shows secondary to primary metal ratio as a function of column density for five runs at $z = 3$. The units on the y-axis is relative and normalized to have the maximum of unity (normally in the densest regions).

metals transported to the lowest density regions with $N_{HI} < 10^{13.5}\text{cm}^{-2}$ are somewhat more recycled through stars than regions at $N_{HI} \sim 10^{13.5}\text{cm}^{-2}$ and originate in higher metallicity systems. This may be explained if the metals are largely transported by winds from galaxies at densest peaks, where relatively more recycling has occurred, whereas near $N_{HI} \sim 10^{13.5}\text{cm}^{-2}$ star formation and enrichment are largely local and recent. Second, increasing the strength of GSW causes more-recycled metals to be transported to low density regions, as expected. Comparison of the two runs with reduced small-scale power (Runs 6,7; long-dashed cyan and dot-dashed magenta curves) and the fiducial run (Run 1, solid red curve) shows that artificial removal of small-scale power thus low mass galaxies significantly reduces the overall values of the ratio of secondary to primary metals of Ly α forest concerned here, while the upturn at the low column density end is preserved. This is of course easily understandable, since much of previous generation of stars can no longer form without the small-scale power. This again highlights the need to have high enough k_{max} in the initial density field.

Finally, Figure 11 shows the mean and median metallicity as a function of density at three redshifts, $z = 2, 3, 4$, with GSW (left panel) and without GSW (right panel). Both runs show only mild evolution in the median metallicity, consistent with observations (Schaye et al. 2003): most of the contamination of the IGM was completed at a relatively high redshift. But the run with GSW shows considerable evolution for the mean metallicity

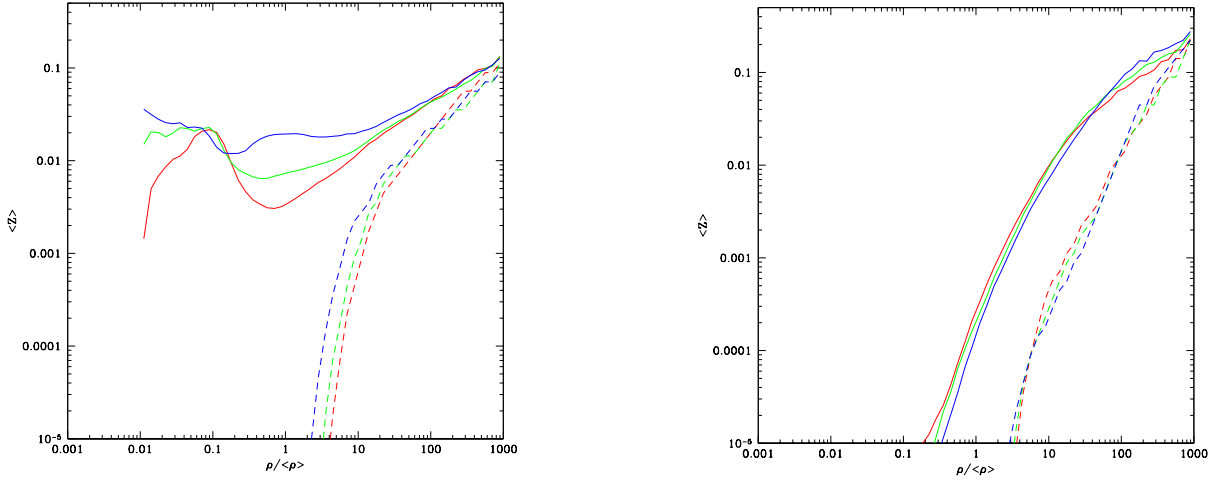


Fig. 11.— shows the mean metallicity (solid curves) and median metallicity (dashed curves) as a function of Ly α cloud column density at redshift $z = 2, 3, 4$ (thick to thin) for Run 1 (N432L11M, left panel) and for Run 2 (N432L11L, right panel).

at $\rho / \langle \rho \rangle < 10$, whereas the run with GSW does not show significant evolution even for the mean metallicity at all densities.

4. Conclusions

We use the latest high mass resolutions hydrodynamic simulation of a Λ CDM model to compute the metallicity evolution of the Ly α forest. Our primary goal is to investigate possible signatures of galactic superwinds on the metallicity of the Ly α forest. There are three main points to be noted.

First, GSW do not significantly alter the flux distribution of Ly α forest and the agreement found in previous simulations of cold dark matter model with observations remains unchanged. On the other hand, GSW do increase the temperature of clouds with column density $N_{HI} < 10^{13.5} \text{cm}^{-2}$, although their contribution to the observed cloud width distribution will be difficult to detect due to large peculiar velocities.

Second, the computed metallicity of Ly α clouds in the column density range of $N_{HI} \sim 10^{14.5} - 10^{15.5} \text{cm}^{-2}$ at $z = 2 - 4$, both with and without GSW, is in reasonable agreement with observations (Schaye et al. 2003). This suggests that these Ly α clouds do not provide a sensitive test of GSW.

Finally, we find a unique signature and sensitive test of GSW, which lies in the still lower density regions with gas density of $\rho/\langle\rho\rangle = 0.01 - 1.0$ and a corresponding column density of $N_{HI} \sim 10^{12} - 10^{14}\text{cm}^{-2}$. Without GSW we predict that both the mean and median metallicity of Ly α clouds in this column density range at $z = 2 - 4$ should have $Z \leq 10^{-3} Z_{\odot}$. With GSW, however, there is a significant fraction ($\sim 25\%$) of Ly α clouds in this column density range which have a high metallicity excess of $10^{-2} Z_{\odot}$, resulting in a mean metallicity of $\sim 10^{-2} Z_{\odot}$. If we (artificially) reduce the number of low mass galaxies ($M \leq 4.5 \times 10^{10} h^{-1} M_{\odot}$), the contamination of the low column density clouds by GSW is reduced by a factor of ~ 4 , so it is likely the mass and metal loss from these low mass systems at $z > 3$ (cf. Dekel & Silk 1986) is the origin of the metals. There is a potential test of this hypothesis. Since reprocessing of metals in these low mass systems is negligible the ratio of secondary (e.g., N) to primary metals (e.g., O,C) is very low and indeed, when we examine this tracer, we find that the ratio of secondary to primary metals is expected to be smaller by a factor of 10 and ≥ 50 for clouds of $N_{HI} \sim 10^{14.5}\text{cm}^{-2}$ and $N_{HI} \leq 10^{13.5}\text{cm}^{-2}$, respectively, compared to that in large galaxies. Thus, future observations of N/O or N/C would help provide an additional test of our proposal. In addition, we find that there is a minimum in the median metallicity for clouds of $N_{HI} \sim 10^{13} - 10^{14}\text{cm}^{-2}$ in the case with GSW, whereas without GSW the metallicity decrease monotonically and rapidly with decreasing column density.

We thank Len Cowie and Piero Madau for useful discussion. This work is supported in part by grants AST-0206299 and NAG5-13381.

REFERENCES

- Adelberger, K. L. 2003, Hubble’s Science Legacy: Future Optical/Ultraviolet Astronomy from Space, ASP Conference Proceedings, Vol. 291, Eds. K. R. Sembach, J. C. Blades, G. D. Illingworth, & R. C. Kennicutt, Jr., p.221 (astro-ph/0210315)
- Adelberger, K. L., Steidel, C. C., Shapley, A. E., & Pettini, M. 2003, ApJ, 584, 45
- Afshordi, N., & Cen, R. 2002, ApJ, 564, 669
- Aguirre, A. 1999, ApJ, 525, 58
- Aguirre, A., Hernquist, L., Schaye, J., Katz, N., Weinberg, D. H., & Gardner, J. 2001, ApJ, 561, 521

- Arnaud, K. A., Mushotzky, R. F., Ezawa, H., Fukazawa, Y., Ohashi, T., Bautz, M. W., Crewe, G. B., Gendreau, K. C., Yamashita, K., Kamata, Y., & Akimoto, F. 1994, *ApJ*, 436, L67
- Arnett, D. 1996, “Supernovae and Nucleosynthesis”, Princeton University Press
- Babul, A., Balogh, M. L., Lewis, G. F., & Poole, G. B. 2002, *MNRAS*, 330, 329
- Balogh, M. L., Babul, A., & Patton, D. R. 1999, *MNRAS*, 307, 463
- Bergeron, J., Aracil, B., Petitjean, P., & Pichon, C. 2002, *A&A*, 396, L11
- Bertschinger, E. 2001, *ApJS*, 137, 1
- Bialek, J. J., Evrard, A. E., & Mohr, J. J. 2001, *ApJ*, 555, 597
- Bland, J., & Tully, B. 1988, *Nature*, 334, 43
- Bond, J. R. & Wadsley, J. W. 1997, Structure and Evolution of the Intergalactic Medium from QSO Absorption Line System, Proceedings of the 13th IAP Astrophysics Colloquium, Paris, Editions Frontieres, p.143 (astro-ph/9710102)
- Borgani, S., Governato, F., Wadsley, J., Menci, N., Tozzi, P., Lake, G., Quinn, T., & Stadel, J. 2001, *ApJ*, 559, L71
- Brighenti, F., & Mathews, W. G. 2001, *ApJ*, 553, 103
- Bromm, V., & Loeb, A. 2003, *Nature*, 425, 812
- Bruzual, A. G. & Charlot, S. 1993, *ApJ*, 405, 538
- Bruzual, A. G. 2000, preprint (astro-ph/0011094)
- Cen, R., & Bryan, G. L. 2001, *ApJ*, 546, L81
- Cen, R., Kang, H., Ostriker, J. P., & Ryu, D. 1995, *ApJ*, 451, 436
- Cen, R., Miralda-Escudé, J., Ostriker, J. P., & Rauch, M. 1994, *ApJ*, 437, L9
- Cen, R., & Ostriker, J. P., 1992, *ApJ*, 399, L113
- Cen, R., & Ostriker, J. P. 1993, *ApJ*, 417, 415
- Cen, R., & Ostriker, J. P. 1999a, *ApJ*, 514, 1
- Cen, R., & Ostriker, J. P. 1999b, *ApJ*, 519, L109

- Cen, R., Ostriker, J. P., Prochaska, J. X., & Wolfe, A. M. 2003, *ApJ*, 598, 741
- Chevalier, R. A., & Clegg, A. W. 1985, *Nature*, 317, 44
- Croft, R. A. C., Weinberg, D. H., Pettini, M., Hernquist, L., & Katz, N. 1999, *ApJ*, 520, 1
- Dahlem, M., Weaver, K. A., & Heckman, T. M. 1998, *ApJS*, 118, 401
- Davé, R., Cen, R., Ostriker, J. P., Bryan, G. L., Hernquist, L., Katz, N., Weinberg, D. H., Norman, M. L., & O’Shea, B. 2001, *ApJ*, 552, 473
- David, L. P., Forman, W., & Jones, C. 1991, *ApJ*, 380, 39
- Dawson, S., Spinrad, H., Stern, D., Dey, A., van Breugel, W., De Vries, W., & Reuland, M. 2002, *ApJ*, 570, 92
- Deharveng, J.-M., Buat, V., Le Brun, B., Milliard, B., Kynth, D., Shull, J. M., & Gry, C. 2001, *A&A*, 375, 805
- Dekel, A., & Silk, J. 1986, *ApJ*, 303, 39
- Della Ceca, R., Griffiths, R. E., Heckman, T. M., Lehnert, M. D., & Weaver, K. A. 1999, *ApJ*, 514, 772
- Dyson, J. E., Arthur, S. J., & Hartquist, T. W. 2002, *A&A*, 390, 1063
- Elizondo, D., Yepes, G., Kates, R., Muller, V., & Klypin, A. 1999a, *ApJ*, 515, 525
- Elizondo, D., Yepes, G., Kates, R., & Klypin, A. 1999b, *NewA*, 4, 101
- Fang, T., & Cen, R. 2004, *astro-ph/0405565*
- Fang, T., Marshall, H. L., Lee, J. C., Davis, D. S., Canizares, C. R. 2002, *ApJ*, 572, L127
- Ferrara, A., Pettini, M. & Shchekinov, Y. 2000, *MNRAS*, 319, 539
- Filippenko, A. V., & Sargent, W. L. W. 1992, *AJ*, 103, 28
- Franx, M., Illingworth, G. D., Kelson, D. D., van Gokkum, P. G., & Tran, K.-V. 1997, *ApJ*, 486, L75
- Gnedin, N. Y. 1998, *MNRAS*, 294, 407
- Gnedin, N. Y., & Ostriker, J. P. 1997, *ApJ*, 486, 581
- Hartquist, T. W., Dyson, J. E., & Williams, R. J. R. 1997, *ApJ*, 482, 182

- Heckman, T. M., Armus, L., & Miley, G. K. 1987, *AJ*, 93, 276
- Heckman, T. M., Robert, C., Leitherer, C., Garnett, D. R., & van der Rydt, F. 1998; *ApJ*, 503, 646
- Heckman, T. M., Sembach, K. R., Meurer, G. R., Leitherer, C., Calzetti, D., & Martin, C. L. 2001, *ApJ*, 558, 56
- Hernquist, L., Katz, N., Weinberg, D. H., & Miralda-Escudé 1996, *ApJL*, 457, L51
- Hultman, J., & Pharasyn, A. 1999, *A&A*, 347, 769
- Hurwitz, M., Jelinsky, P., & Dixon, W. V. D. 1997, *ApJ*, 481, L31
- Kaiser, N. 1991, *ApJ*, 383, 104
- Katz, N., Hernquist, L., & Weinberg, D. H. 1996, *ApJS*, 105, 19
- Katz, N., Hernquist, L., & Weinberg, D. H. 1992, *ApJ*, 399, L109
- Kay, S. T., Pearce, F. R., Frenk, C. S., & Jenkins, A. 2002, *MNRAS*, 330, 113
- Koo, B.-C., & McKee, C.F. 1992a, *ApJ*, 388, 93
- Koo, B.-C., & McKee, C.F. 1992b, *ApJ*, 388, 103
- Lehnert, M. D., & Heckman, T. M. 1996, *ApJ*, 462, 651
- Lloyd-Davies, E. J., Ponman, T. J., & Cannon, D. B. 2000, *MNRAS*, 315, 689
- Loewenstein, M. 2000, *ApJ*, 532, 17
- Mac Low, M.-M., & Ferrara, A. 1999, *ApJ*, 513, 142
- Madau, P., Ferrara, A., & Rees, M. J. 2001, *ApJ*, 555, 92
- Marlowe, A. T., Heckman, T. M., Wyse, R. F. G., & Schommer, R. 1995, *ApJ*, 438, 563
- Martin, C. L. 1999, *ApJ*, 513, 156
- Martin, C. L., Kobulnicky, H. A., & Heckman, T. M. 2002, *ApJ*, 574, 663
- Mathur, S., Weinberg, D. H., & Chen, X. 2003, *ApJ*, 582, 82
- McCarthy, P. J., Heckman, T. M., & van Breugel, W. 1987, *AJ*, 93, 264
- McCarthy, I. G., Babul, A., & Balogh, M. L. 2002, *ApJ*, 573, 515

- McDonald, P., Miralda-Escudé, J., Rauch, M., Sargent, W. L. W., Barlow, T. A., Cen, R., & Ostriker, J. P. 2000, *ApJ*, 543, 1
- McKee, C. F. & Ostriker, J. P. 1977, *ApJ*, 218, 148
- Metzler, C. A. & Evrard, A. E. 1994, *ApJ*, 437, 564
- Miralda-Escudé, J., Cen, R., Ostriker, J. P., & Rauch, M. 1996, *ApJ*, 471, 582
- Mori, M., Ferrara, A., & Madau, P. 2002, *ApJ*, 571, 40
- Mushotzky, R. F., & Lowenstein, M. 1997, *ApJ*, 481, L63
- Mushotzky, R. F., Lowenstein, M., Arnaud, A. K., Tamura, T., Fukazawa, Y., Matsushita, K., Kikuchi, K., & Hatsukade, I. 1996, *ApJ*, 466, 686
- Nagamine, K. 2002, *ApJ*, 564, 73
- Nagamine, K., Springel, V., Hernquist, L., & Machacek, M. 2004a, *MNRAS*, 350, 385
- Nagamine, K., Cen, R., Hernquist, L., Ostriker, J. P., & Springel, V. 2004b, *ApJ*, submitted (astro-ph/0406032)
- Nath, B. B., & Trentham, M. 1997, *MNRAS*, 291, 505
- Navarro, J. F., Frenk, C. S., & White, S. D. M. 1995, *MNRAS*, 275, 720
- Neumann, D. M., & Arnaud, M. 2001, *A&A*, 373, L33
- Nicastro, F., et al. 2002, *ApJ*, 573, 157
- Norman, M. L., O’Shea, B. W., & Paschos, P. 2004, *ApJ*, 601, L115
- Ostriker, J. P., & Cowie, L. L. 1981, *ApJ*, 243, L127
- Papaderos, P., Fricke, K. J., Thuan, T. X., & Loose, H.-H. 1994, *A&A*, 291, L13
- Pen, U.-L. 1999, *ApJ*, 510, L1
- Pettini, M., Kellogg, M., Steidel, C. C., Dickinson, M., Adelberger, K. L., & Giavalisco, M. 1998, *ApJ*, 508, 539
- Pettini, M., Shapley, A. E., Steidel, C. C., Cuby, J.-G., Dickinson, M., Moorwood, A. F. M., Adelberger, K. L., & Giavalisco, M. 2001, *ApJ*, 554, 981

- Pettini, M., Rix, S. A., Steidel, C. C., Adelberger, K. L., Hunt, M. P., & Shapley, A. E. 2002, *ApJ*, 569, 742
- Ponman, T. J., Cannon, D. B., & Navarro, J. F. 1999, *Nature*, 397, 135
- Press, W. H., Rybicki, G. B., & Schneider, D. P. 1993, *ApJ*, 414, 64
- Rauch, M., Miralda-Escudé, J., Sargent, W. L. W., Barlow, T. A., Weinberg, D. H., Hernquist, L., Katz, N., Cen, R., & Ostriker, J. P. 1997, 489, 7
- Raymond, J. C., Cox, D. P., & Smith, B. W. 1976, *ApJ*, 204, 290
- Ricotti, M., & Ostriker, J. P. 2004, *MNRAS*, 350, 539
- Ritchie, B. W., & Thomas, P. A. 2001, *MNRAS*, 323, 743
- Rupke, D. S., Veilleux, S., & Sanders, D. B. 2002, *ApJ*, 570, 588
- Ryu, D., Ostriker, J. P., Kang, H., & Cen, R. 1993, *ApJ*, 414, 1
- Sazonov, S. Y., Ostriker, J. P., & Sunyaev, R. A. 2004, *MNRAS*, 347, 144
- Scannapieco, E., Ferrara, A., & Madau, P. 2002, *ApJ*, 574, 590
- Scannapieco, E., Thacker, R. J., & Davis, M. 2001, *ApJ*, 557, 605
- Schaye, J., Aguirre, A., Kim, T.-S., Theuns, T., Rauch, M., & Wallace, W. L. W. 2003, *ApJ*, 596, 768
- Schwarz, J., Ostriker, J. P., & Yahil, A. 1975, *ApJ*, 202, 1
- Smith, S. J. 1996, *ApJ*, 473, 773
- Songaila, A., & Cowie, L. L. 1996, *AJ*, 112, 335 (SC96)
- Spergel, D. N. et al. 2003, *ApJS*, 148, 175
- Springel, V., & Hernquist, L. 2003, *MNRAS*, 339, 289
- Steinmetz, M. 1996, *MNRAS*, 278, 1005
- Strickland, D. K., & Stevens, I. R. 2000, *MNRAS*, 314, 511
- Suchkov, A. A., Berman, V. G., Heckman, T. M., & Balsara, D. S. 1996, *ApJ*, 463, 528
- Thacker, R. J., Scannapieco, E., & Davis, M. 2002, *ApJ*, 581, 836

- Theuns, T., Leonard, A., Efstathiou, G., Pearce, F. R., & Thomas, P. R. 1998, *MNRAS*, 301, 478
- Theuns, T. T., Viel, M., Kay, S., Schaye, J., Carswell, R. F., & Tzanavaris, P., 2002, *ApJ*, 578, L5
- Tozzi, P., & Norman, C. 2001, *ApJ*, 546, 63
- Tripp, T. M., Savage, B. D., & Jenkins, E. B. 2000, *ApJ*, 534, L1
- Tytler, D., Fan, X.-M., Burles, S., Cottrell, L., Davis, C., Kirkman, D., & Zuo, L. 1995, in *QSO Absorption Lines*, ed. G. Meylan (Berlin: Springer), 289
- Veilleux, S., Bland-Hawthorn, J., Cecil, G., Tully, R. B., & Miller, S. T. 1999, *ApJ*, 520, 111
- Veilleux, S., Shopbell, P. L., & Miller, S. T. 2001, *AJ*, 121, 198
- Voit, G. M. & Bryan, G. L. 2001, *Nature*, 414, 425
- Voit, G. M., Bryan, G. L., Balogh, M. L., Bower, R. G., 2002, *ApJ*, 576, 601
- White, M., Hernquist, L., & Springel, V. 2002, *ApJ*, 579, 16
- White, R. E., III 1991, *ApJ*, 367, 69
- Woosley, S. E., & Weaver, T. A. 1995, *ApJS*, 101, 181
- Wu, K. K. S., Fabian, A. C., & Nulsen, P. E. J. 2000, *MNRAS*, 318, 889
- Yepes, G., Kates, R., Khokhlov, A., & Klypin, A. 1997, *MNRAS*, 284, 235
- Yoshida, M., Taniguchi, Y., & Murayama, T. 1999; *AJ*, 117, 1158
- Zhang, Y., Anninos, P., & Norman, M. L. 1995, *ApJL*, 453, L57